Nonlinear Negative Stiffness Wing-Tip Spring Device for Gust Loads Alleviation

A. Castrichini[1], J.E. Cooper[2]
University of Bristol, Bristol, BS8 1TH, United Kingdom

T. Wilson[3]
Airbus Operations Ltd., Filton, BS99 7AR, United Kingdom

A. Carrella[4], Y. Lemmens[5]
Siemens PLM Software, Leuven, Interleuvenlaan 68 B-3001, Belgium

A recent consideration in aircraft design is the use of folding wing-tips with the aim of enabling higher aspect ratio configurations with less induced drag whilst also meeting airport gate limitations. This study builds on previous work investigating the effect of exploiting the folding wing-tips in-flight as a device to reduce dynamic gust loads, but now with the introduction of a passive nonlinear negative stiffness hinge spring. A single degree of freedom model and a representative civil jet aircraft aeroelastic model were used to investigate the dynamic gust response for different hinge device designs. It was found that significant reductions in the dynamic loads were possible.

Nomenclature

Symbols

b_l	=	Aerodynamic lag-pole
c	=	Mean chord
d_{cg}	=	Center of gravity/hinge line distance
D	=	Damping matrix
D_θ	=	Damping coefficient
H	=	Gust gradient
I_θ	=	Moment of inertia
F_{Aero}	=	Aerodynamic forces vector
k	=	Reduced frequency
K	=	Stiffness matrix
$K_{()}$	=	Hinge stiffness
K_o	=	Oblique spring stiffness
K_θ	=	Torsional spring stiffness
L	=	Oblique spring length
L_g	=	Gust length
m	=	Wing-tip mass
M	=	Mass matrix
$M_{()}$	=	Hinge moment
q_{dyn}	=	Dynamic pressure
q_f	=	Modal coordinates
$Q_{()}$	=	Generalized aerodynamic force matrices
Q_e	=	External forces
$Q_{i()}$	=	Coefficient matrices of RFA
Q_v	=	Quadratic velocity forces

[1] PhD Student, Dept. of Aerospace Engineering
[2] Airbus Royal Academy of Engineering Sir George White Professor of Aerospace Engineering, AFAIAA
[3] Head of Technical Capability for Aircraft Loads Flight Physics
[4] Product Manager Test, Test Division
[5] Project Leader RTD, Aerospace Competence Centre

r = Pulley radius
R = Body reference translation
R_l = Aerodynamic states vector
V = True air speed
w = Gust vector
w_g = Gust velocity
w_{g0} = Peak of the gust velocity
w_{ref} = Reference gust velocity
x_0 = Gust origin position
x_j = j^{th} panel's control node position
α = Angle of attack
γ = Oblique spring aspect ratio
γ_j = j^{th} panel's dihedral angle
δ = Aerodynamic control surfaces vector
θ = Wing-tip folding angle
Λ = Hinge orientation angle
ξ = Generalized coordinates vector
σ = Oblique spring angle
ν = Springs stiffness ratio
Ψ = Body reference rotation

Superscript
$\hat{}$ = Nondimensional quantities
$\dot{}$ = Differentiation with respect to time
$\tilde{}$ = Fourier transform
$\bar{}$ = Generalized variable

Subscript
0 = Initial value

I. Introduction

Much effort has been made to design aircraft in order to optimize fuel consumption through the reduction of aerodynamic drag. A sizable contribution to the overall drag is lift-induced drag, which can be reduced by increasing the wingspan, but such a design solution has well defined limits imposed by the maximum aircraft dimensions allowed at airports and also the resulting increase in bending moments along the wing. A possible solution to the first issue is the use of folding wings that can be employed on the ground in a similar way to the retractable wings used on aircraft carrier borne aircraft. An example of this approach relevant to civil applications is the latest version of the B-777 which will have a folding wing capability to be activated during taxiing to and from the gates. The inclusion of such a design feature raises the question as to whether folding devices could also be used to enable loads reduction on the aircraft during the flight [1].

This work is aimed at studying the benefits of using a flexible wing-fold device for loads alleviation and considering how it would be implemented on civil jet aircraft. The main idea consists of introducing a hinge in order to allow the wing-tips (WT) to rotate, as shown in Fig. 1. The orientation of the hinge line relative to the direction of travel of the aircraft is a key parameter to enable successful loads alleviation [1]. When the hinge line is not parallel to the free stream, but is rotated outboard as in Fig. 1(b, d), folding the wing-tip decreases the local angle of attack α which can be defined in terms of hinge orientation Λ and angle of rotation of the wing-tip θ as

$$\alpha = -\tan^{-1}(\tan\theta \sin\Lambda) \tag{1}$$

This equation implies that the hinge angle provides a means to reduce the loads acting on the wing through downwash at the wing-tip.

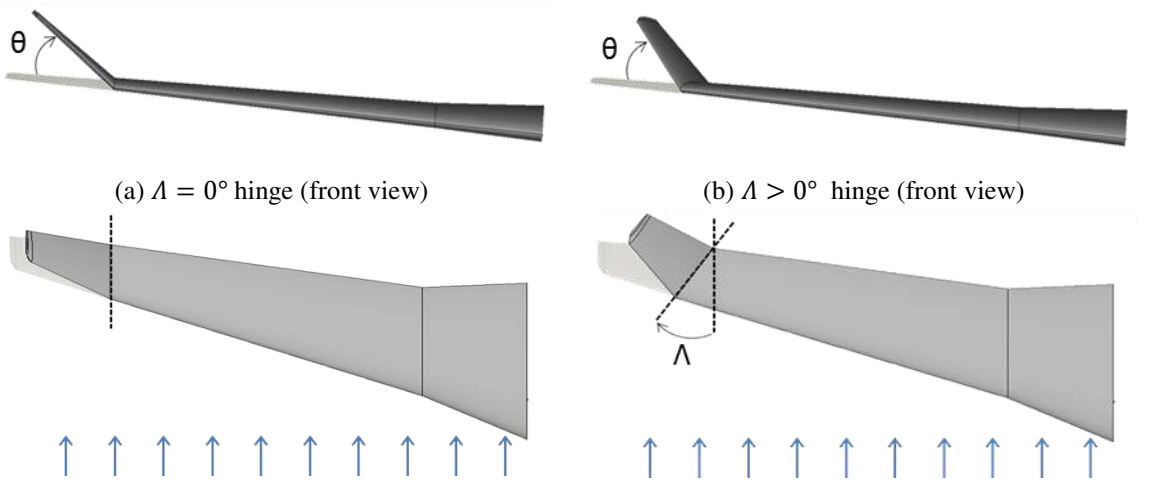

(a) $\Lambda = 0°$ hinge (front view)

(b) $\Lambda > 0°$ hinge (front view)

(c) $\Lambda = 0°$ hinge (top view)

(d) $\Lambda > 0°$ hinge (top view)

Figure 1. Hinge Orientations

Previous work [1] considered several structural configurations for the loads alleviation device, varying the hinge direction, wing-tip weight, linear hinge spring stiffness and linear hinge damping value for static and dynamic gust loads. Figure 2 shows the aeroelastic model used for the analyses, which was a modified version of the FFAST aeroelastic model [2] of a representative civil jet aircraft, whose structure was modelled using a "stick" model with lumped masses and the aerodynamic forces determined using the doublet lattice panel method. The main objective was to investigate the possibility of increasing the aspect ratio whilst limiting the increase in loads (especially in terms of wing bending moment), thus keeping the structure as light as possible. A baseline model, without wing-tips, Fig. 2, was considered as the reference to evaluate the use of folding wing-tips, also shown in Fig. 2, which were attached to the structure using a flexible hinge, giving a span increase of 25% compared to the baseline model. Figure 3 shows a detailed view of the structural model with the attached wing-tip device. Significant reductions in the resulting loads were achieved with a passive linear hinge device for small hinge stiffness, no hinge damping, reduced wing-tip weight and swept hinge.

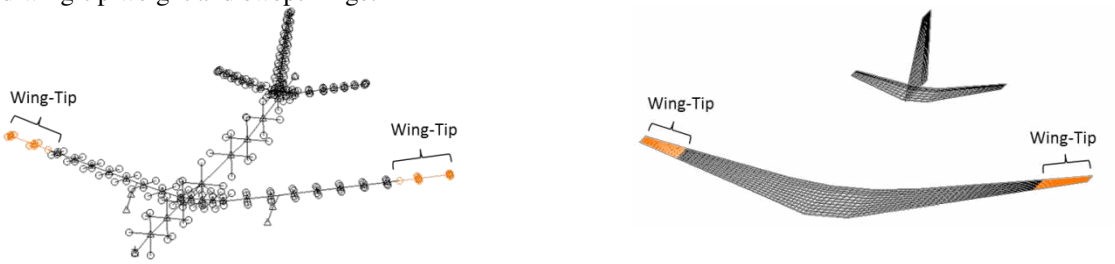

(a) Structural model

(b) Aerodynamic model

Figure 2. Aeroelastic Model Showing Baseline Model and Wing-Tips

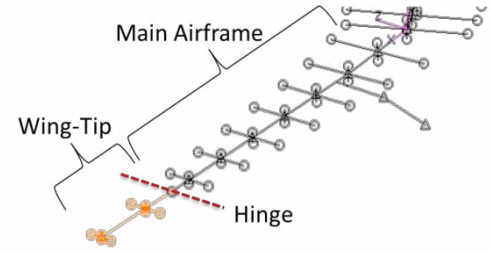

Figure 3. Folding Wing-Tip Modeling Detail

Previous research has shown [1] that a quick response of the wing-tip to the gust is essential for achieving an efficient loads reduction; the phase shift between the wing root bending moment (WRBM) and the folding angle should be as small as possible to let the wing-tip alleviate the loads. Significant reductions in the resulting loads were achieved with a passive linear hinge device for small hinge stiffness, no hinge damping, reduced wing-tip weight and swept hinge. However, having such a small hinge stiffness value means that the wing-tip will deflect during straight and level cruise flight due to the static trim loads; an undesirable effect that will be detrimental to the aerodynamic performance and trim behavior. Ideally, the wing-tip should not deflect during cruise, but only operate once a gust is encountered. With a linear hinge device there is a conflict between having a low spring stiffness for good gust loads alleviation and a high spring stiffness to counteract static trim deflections. Consequently, a compromise in the design needs to be found in order to maximize the benefits of gust alleviation whilst avoiding motion during cruise which means that sub-optimal performance is achieved.

Gatto et. al. [4] proposed the using of a composite winglet characterized by two stable configurations: under the effect of the aerodynamic loads the structure would have snapped toward a new stable configuration that generated lower aerodynamic loads, but such design did not allow to recover the original stable configuration. Furthermore the lack of a control of the "snap-through" process led to a significant dynamic loading during the passage between stable configurations. Arrieta, Bilgen et al. [5, 6] addressed the problem of the implementation of the "snap-through" process by using piezoelectric actuators in order to excite the bending resonant frequencies at the different stable configurations of a clamped wing-tip model, resulting in a good control capability even under the effect of external aerodynamic loads.

This paper builds upon previous work [1, 3] that considered linear and nonlinear hinge devices. An investigation is made into the use of a passive negative stiffness nonlinear hinge for the folding wing-tip concept to improve the gust loads alleviation capability. The proposed hinge device is a modified version of the high static low dynamic stiffness (HSLD) mechanism studied by Carrella et al. [7]. The nonlinear spring device needs to be stiff enough to allow the wing-tip not to deflect during the cruise, whilst allowing significant rotations when significant gust events are encountered. In this way, significant wing-tip deflections are achieved when the aerodynamic loads are higher than some given threshold, allowing efficient loads alleviation. A series of preliminary numerical simulations are performed using a single degree of freedom model and a representative civil jet aircraft aeroelastic model to investigate the influence of the design parameters on the dynamic response of the nonlinear aeroelastic systems to gusts.

II. Nonlinear Hinge Device

A. Mathematical Modeling

Nonlinear stiffness mechanisms are widely used as passive vibration isolators [7-10]. These kind of mounts are characterized by a high static low dynamic stiffness behavior; they are able to support a given mass (high static stiffness) while having at the same time a very low natural frequency (low dynamic stiffness) which is necessary for the vibration isolation purposes.

Several variants of nonlinear mounts have been proposed in the literature [11]; Carrella et al. [7] have provided a rigorous and analytic static investigation of a particular configuration given by a combination of a vertical spring connected in parallel with two oblique springs.

In this paper a torsional variant of the mechanism proposed by Carrella [7] was used; the nonlinear hinge device was achieved by combining a linear torsional spring, K_θ in parallel with two linear oblique springs K_o as shown in Fig. 4. Furthermore, a pulley was introduced to convert the axial forces provided by the oblique springs into a torque applied on the hinge line.

When only the oblique springs are employed, the resulting moment on the wing-tip hinge is given by

$$M_{nl} = 2K_o r(L_0 - L)\sin\sigma \tag{2}$$

where L is the length of the oblique springs, σ is the angle of inclination of the oblique springs, K_o is the related linear stiffness and r is the radius of the pulley. By consideration of the geometry, $\sin\sigma = \frac{h_0 - r(\theta-\theta_0)}{L}$; $L = \sqrt{(h_0 - r(\theta-\theta_0))^2 + a^2}$; $L_0 = \sqrt{h_0^2 + a^2}$ and the non-dimensional parameters $\gamma = \frac{a}{L_0} = \cos\sigma_0$ and $\hat{r} = \frac{r}{L_0}$; the nonlinear moment given by the oblique springs can be expressed as

$$M_{nl} = K_o r^2 \widehat{M}_{nl}$$
$$= K_o r^2 \frac{2}{\hat{r}}\left(\sqrt{1-\gamma^2} - \hat{r}(\theta-\theta_0)\right)\left[\left(\hat{r}^2(\theta-\theta_0)^2 - 2\sqrt{1-\gamma^2}\hat{r}(\theta-\theta_0)+1\right)^{-1/2} - 1\right] \quad (3)$$

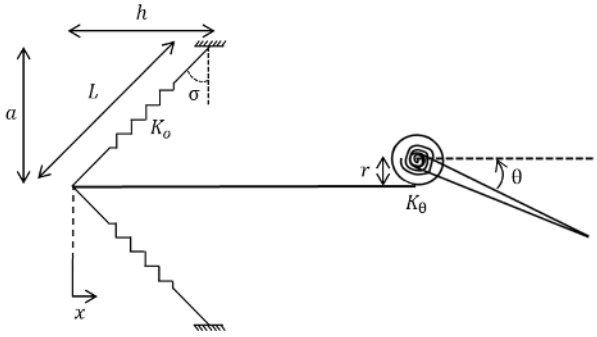

Figure 4. Schematic Representation of the Nonlinear Spring Device

The non-dimensional parameters γ and $\hat{r}$ define the geometry of the nonlinear device where γ is the aspect ratio of the oblique springs; when $\gamma = 0$ the springs are initially horizontal, whilst for $\gamma = 1$ the springs are initially vertical. $\hat{r}$ represents the aspect ratio of the pulley with respect to the oblique springs initial length; the higher that $\hat{r}$ is, the greater the longitudinal displacement of the oblique springs x for a given wing-tip rotation.

Such a configuration is characterized by three equilibrium points when $\widehat{M}_{nl}(\theta) = 0$, given by

$$\theta_1^{eq} = \theta_0; \qquad \theta_2^{eq} = \frac{\sqrt{1-\gamma^2}}{\hat{r}} + \theta_0; \qquad \theta_3^{eq} = 2\frac{\sqrt{1-\gamma^2}}{\hat{r}} + \theta_0 \quad (4)$$

and note that θ_1^{eq} and θ_3^{eq} are symmetric with respect θ_2^{eq} due to the symmetry of the nonlinear device, as shown in Figure 5.

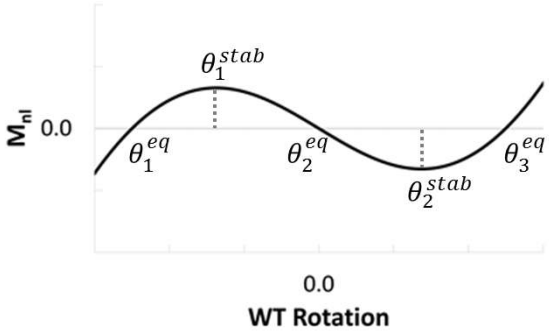

Figure 5. Oblique Springs Equilibrium Points

The related non-dimensional stiffness is evaluated by differentiating $\widehat{M}_{nl}$ with respect to the angle of rotation θ as

$$\widehat{K}_{nl} = \frac{K_{nl}}{K_o} = \frac{d\widehat{M}_{nl}}{d\theta} = 2\left[1-\gamma^2\left(\hat{r}^2(\theta-\theta_0)^2 - 2\sqrt{1-\gamma^2}\hat{r}(\theta-\theta_0)+1\right)^{-3/2}\right] \quad (5)$$

The stiffness $\widehat{K}_{nl}$ is zero for

$$\theta_{1,2}^{stab} = \theta_2^{eq} \pm \frac{\sqrt{\gamma^{4/3}-\gamma^2}}{\hat{r}} \quad (6)$$

which defines the stability boundaries of the nonlinear springs. The interval $(\theta_1^{stab}; \theta_2^{stab})$, shown in Figure 5, represents the unstable branch of the nonlinear moment curve $\widehat{M}_{nl}(\theta)$ where $\widehat{K}_{nl}$ is negative, i.e. the springs would provide a hinge moment in the folding angle direction.

When $\gamma = 1$, there is only one equilibrium point and $\theta_{1,2,3}^{eq} = \theta_{1,2}^{stab} = \theta_0$; for $\gamma < 1$ all the points are distinct and $\theta_1^{eq} < \theta_1^{stab} < \theta_2^{eq} < \theta_2^{stab} < \theta_3^{eq}$and therefore θ_1^{eq} and θ_3^{eq} are stable equilibrium points characterized by a positive stiffness value, while θ_2^{eq} is unstable being $\widehat{K}_{nl}\left(\theta_2^{eq}\right) < 0$. The latter condition represents the configuration when the oblique springs are vertical.

When a linear torsional spring K_θ is put in parallel with the oblique springs, the overall structural moment and stiffness are given by

$$M_{struct} = K_\theta \widehat{M}_{struct} = K_\theta\left[(\theta - \theta_0) + \nu\widehat{M}_{nl}\right] = K_\theta\left(\widehat{M}_l + \nu\widehat{M}_{nl}\right) \tag{7}$$

$$K_{struct} = K_\theta \frac{d\widehat{M}_{struct}}{d\theta} = K_\theta\left(1 + \nu\widehat{K}_{nl}\right) \tag{8}$$

where $\nu = \frac{K_o r^2}{K_\theta}$ is the ratio of the equivalent torsional stiffness of the oblique springs, $K_o r^2$, to the linear torsional spring K_θ.

Figure 6 shows the effects on the non-dimensional structural hinge moment $\widehat{M}_{struct}$ and stiffness $\widehat{K}_{struct}$ of the design parameter $\gamma,\ \hat{r}, \nu$. The characteristic "S" shape of the nonlinear moment curve is due to the nonlinearity introduced by the oblique springs; for $\theta_1^{stab} < \theta < \theta_2^{stab}$ these provide a negative stiffness contribution that can overcome the positive stiffness of the linear spring for a given rotation θ. This nonlinear effect is a function of the geometry of the system $\gamma,\ \hat{r}$ and the stiffness ratio value ν. For $\gamma = 0$ the springs are initially horizontal, while they are initially vertical for $\gamma = 1$. The lower that γ is, the more the oblique springs absorb potential energy during the wing-tip rotation, which is then released through the nonlinear "snap through" mechanism of the oblique springs once it becomes dominant. The higher that $\hat{r}$ is, the smaller the interval $\Delta\theta$ in which the oblique springs provide a negative stiffness contribution as $\theta_{1,2}^{stab} \propto \hat{r}^{-1}$. The higher that the stiffness ratio is, the higher the contribution of the oblique springs over the linear torsional spring, but since it does not affect $\theta_{1,2}^{stab}$, as shown in Eq. (6), the range of rotation over which the oblique springs provide a negative stiffness contribution does not change with ν.

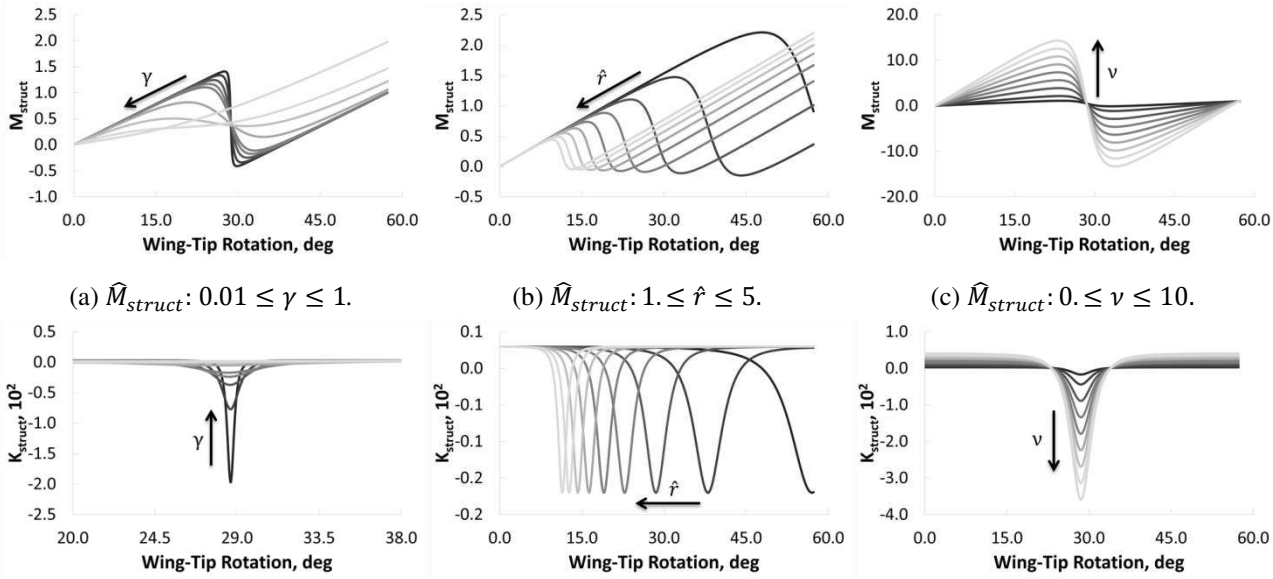

(a) $\widehat{M}_{struct}$: $0.01 \le \gamma \le 1.$ (b) $\widehat{M}_{struct}$: $1. \le \hat{r} \le 5.$ (c) $\widehat{M}_{struct}$: $0. \le \nu \le 10.$

(d) $\widehat{K}_{struct}$: $0.01 \le \gamma \le 1.$ (e) $\widehat{K}_{struct}$: $\hat{r} = 1. \le \hat{r} \le 5.$ (f) $\widehat{K}_{struct}$: $\nu = 0. \le \nu \le 10.$

Figure 6. Nonlinear Moment and Stiffness Curves

When the oblique springs are combined with a linear torsional spring, it is not possible to have a closed form formulation of the equilibrium points of the system as a function of the design parameters. A bifurcation analysis was performed to investigate the dependency of the number of the equilibrium points with γ, $\hat{r}$ and ν. Figure 7 shows the bifurcation diagram of the mechanical system and it has been found that the number of the equilibrium points is solely a function of the $\gamma - \nu$ combination, while $\hat{r}$ did not have any effect. The system exhibited a bistable behavior in the grey region in Fig. 7, being characterized by three equilibrium points (2 stable and 1 unstable), while the white region allowed only one stable equilibrium point.

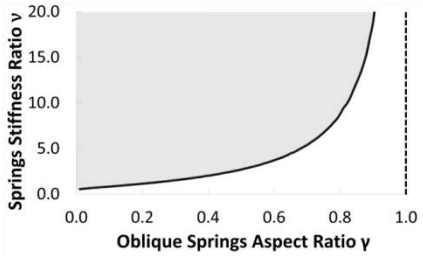

Figure 7. Bifurcation Diagram (grey region: 3 equilibrium points; white region: 1 equilibrium point)

B. High Static Low Dynamic Aeroelastic Stiffness Design

When the overall aeroelastic system is considered, the hinge device stiffness is characterized not only by the positive stiffness provided by the linear torsional spring and the negative stiffness, for $\theta_1^{stab} < \theta < \theta_2^{stab}$, of the oblique springs, but also by a positive stiffness contribution due to the aerodynamic forces for $\Lambda > 0$. For an outboard rotated hinge sweep angle, an upward wing-tip deflection produces a decrease in the local angle of attack leading to the generation of incremental aerodynamic forces that oppose the wing-tip deflection.

The concept behind a high static and low dynamic aeroelastic stiffness hinge mechanism is to design a spring that is stiff enough to keep the wing-tip trimmed during cruise, but then to take advantage of the negative stiffness capability provided by the oblique springs in order to allow a rapid rotation of the folding wing-tip during a gust event; the device should also be able to return to an undeflected configuration after the gust event. Figure 8 shows the schematic operation of the device. The wing-tip is attached to the springs with an initial downwards deflection angle when no aerodynamic forces are applied. At the trim flight configuration, the aerodynamic forces generate a rotation of the wing-tip, the oblique springs would then be compressed to assume a vertical configuration and the static load would be taken mainly by the linear torsional spring. In such a configuration, the oblique springs would not generate any moment, but they would provide a negative stiffness contribution that, counteracting the positive structural and aerodynamic moments, would allow a rapid deflection of the wing-tip in the case of a gust event. The negative aerodynamic forces generated by the upward rotation would lead the system to move to the original position.

The overall static aeroelastic hinge moment and stiffness can be expressed as

$$M_{tot} = M_{struct} - K_{aero\theta}\theta - M_{ext} \tag{9}$$

$$K_{tot} = K_{struct} - K_{aero\theta} \tag{10}$$

where M_{struct} and K_{struct} are the structural moment and stiffness, respectively, given by the linear and nonlinear springs combination as in Eqs. (7) and (8), $K_{aero\theta}$ is the wing-tip aerodynamic stiffness that defines the hinge moment contribution due to the aerodynamic forces generated by the wing-tip deflection and M_{ext} represents the overall hinge moment due to the combination of the external static loads, such as the aerodynamic trim loads or the gravitational loads.

In order to let the hinge device behave with a high static low dynamic aeroelastic spring stiffness, it is required that the wing-tip was undeflected at the horizontal trimmed flight condition. Assuming as known the overall static external moments acting on the hinge, and assuming that no oblique springs are employed, the value of the linear spring stiffness that satisfies the $\theta_{trim} = 0°$ condition is given by

$$K_\theta = \frac{M_{ext}}{\theta_0} \tag{11}$$

It is essential that introducing the oblique springs does not generate any variation of the equilibrium point defined for the linear system. This is achieved by designing the nonlinear springs in order to not provide any moment at the static equilibrium point, which infers $\theta_2^{eq} = \theta_{trim} = 0°$. From Eq. (4), this condition leads to the definition of the non-dimensional radius as

$$\hat{r} = \frac{\sqrt{1-\gamma^2}}{\theta_0} \tag{12}$$

for any given values of θ_0 and γ. When Eq. (12) is satisfied, the equilibrium point of the nonlinear system does not change by varying the stiffness of the oblique springs, since in Eq. (4) it has been shown that θ_2^{eq} (and so θ_{trim}) is not a function of ν. Therefore, the oblique spring stiffness can be used as a tuning parameter to calibrate the overall stiffness of the hinge device around the equilibrium point as shown in Fig. 9. When Eq. (10) is evaluated at $\theta_{trim} = 0°$ and set to zero, this achieves a "quasi-zero-aeroelastic-stiffness" at the equilibrium point. The spring stiffness ratio to achieve this effect is given by

$$\nu_{qzas} = \frac{\gamma(1+\nu_{aero})}{2(1-\gamma)} \tag{13}$$

where $\nu_{aero} = \frac{K_{aero\theta}}{K_\theta}$ is the ratio of the torsional aerodynamic stiffness, $K_{aero\theta}$, to the linear torsional spring K_θ.

A value of $\nu < \nu_{qzas}$ would allow the system to have only one stable equilibrium point, while $\nu > \nu_{qzas}$ would lead to three possible equilibrium points, of which $\theta_{trim} = 0°$ is unstable due to the negative aeroelastic stiffness K_{tot}. If Eq. (8) is evaluated at $\theta_{trim} = 0°$ and the structural stiffness is set to zero, the value of the spring stiffness ratio that leads to a "quasi-zero-structural-stiffness" [7] is given by

$$\nu_{qzss} = \frac{\gamma}{2(1-\gamma)} \tag{14}$$

When Eqs. (11) and (12) are satisfied and $\nu_{qzss} \leq \nu \leq \nu_{qzas}$, the hinge device behaves as a high static low dynamic aeroelastic stiffness device exhibiting only one equilibrium point, a negative structural stiffness and a positive aeroelastic stiffness. Figures 8 and 9 shows the typical $M_{tot}(\theta)$ trend for a high static low dynamic aeroelastic stiffness design.

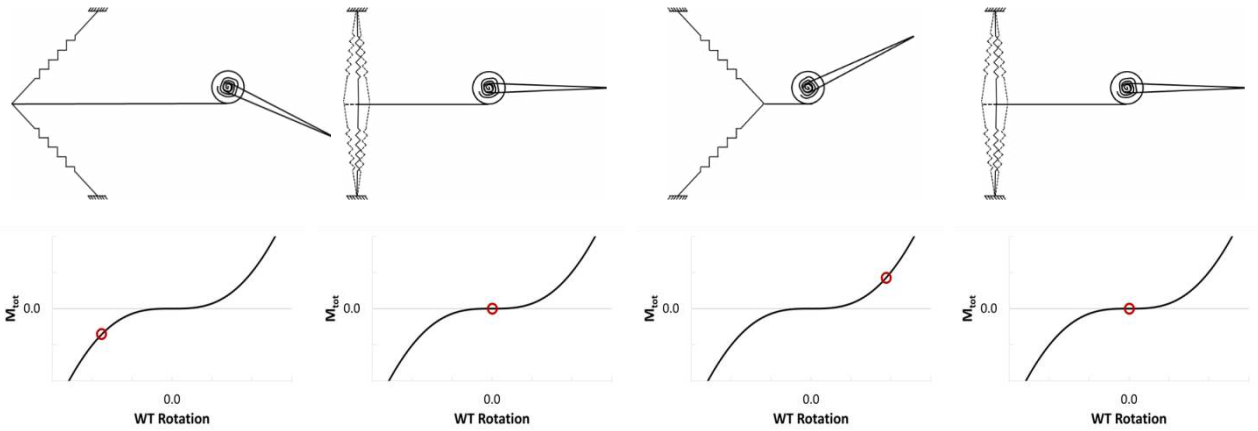

(a) Initial deflection (b) Trim configuration (c) Gust deflection (d) Trim configuration

Figure 8. Schematic of Wing-Tip Operation

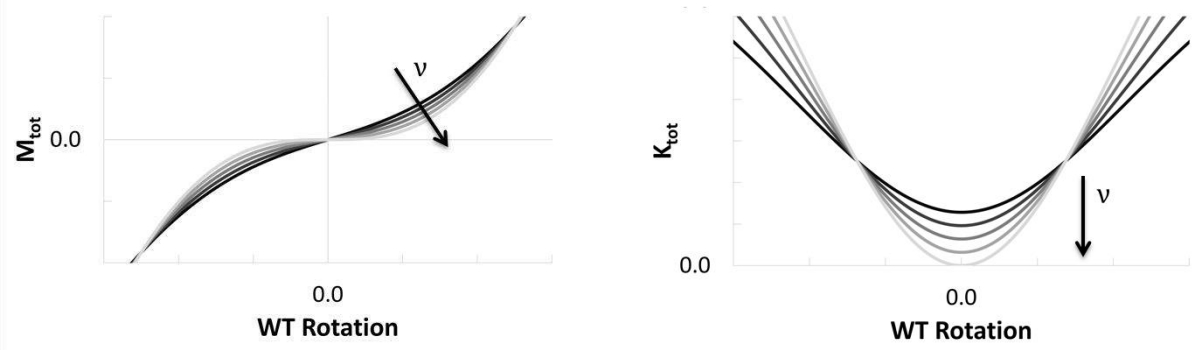

(a) Total aeroelastic hinge moment (b) Total aeroelastic hinge stiffness

Figure 9. M_{tot} and K_{tot} Calibration by Varying the Oblique Spring Stiffness

III. Single Degree of Freedom Model

The high static low dynamic aeroelastic stiffness hinge device, introduced in the previous section, is applied here to a single degree of freedom model in order to gain an understanding of the isolated dynamic response of such a device when no structural dynamic coupling with the main airframe occurs.

A. Structural Modelling

Figure 10(a) shows the structural model used for the analyses, comprising a rigid stick structural model with lumped masses. The wing-tip preserves the same geometry and mass distribution of the $100\,Kg$ folding devices considered previously [1]. The structural model has only one degree of freedom given by the rigid rotation around a hinge axis at the wing-tip root and the nonlinear torsional spring is defined at the hinge.

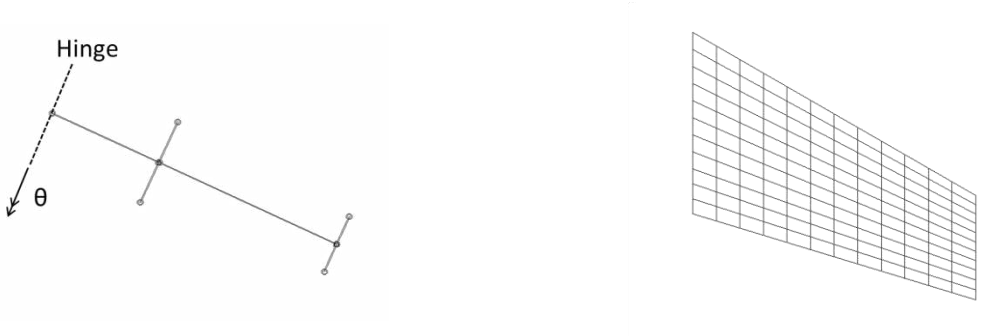

(a) Structural model (b) Aerodynamic model

Figure 10. SDOF Wing-Tip Aeroelastic Model (top view)

B. Aerodynamic Modelling

The wing-tip aerodynamic mesh is shown in Fig. 10(b), where the doublet lattice method [12, 13] was employed to model the hinge moment due to the aerodynamic forces which, in the frequency domain, is defined as

$$M_{aero} = q_{dyn}[Q\tilde{\theta} + Q_g\tilde{w}] \tag{15}$$

where $Q_{(1\,X\,1)}$ and $Q_{g(1\,X\,N_{Panels})}$ are the generalized aerodynamic forces matrices related to the Fourier transform of the generalized coordinate $\tilde{\theta}$ and the gust vector $\tilde{w}$. The latter term defines the downwash on a generic aerodynamic panel *j* due to the gust such that

$$w_j = \cos\gamma_j \frac{w_{g0}}{2V}\left(1-\cos\left(\frac{2\pi V}{L_g}\left(t-\frac{x_0-x_j}{V}\right)\right)\right) \tag{16}$$

where L_g is the gust length (twice the gust gradient *H*), V is the true air speed and w_{g0} peak gust velocity. The latter defined (in m) as [14]

$$w_{g0} = w_{ref}\left(\frac{H}{106.17}\right)^{\frac{1}{6}} \tag{17}$$

The Doublet Lattice panel method is based upon linear unsteady potential flow theory, making the assumptions of inviscid, irrotational, compressible and attached flow, subject to small angle of attack or side slip. As a consequence, nonlinear aerodynamic effects such as flow separations, shocks, turbulence, boundary layers as well as aerodynamic drag were not accounted for. Only the lift forces and pitching moment, defined for each aerodynamic panel, were considered in the aerodynamic loads estimation. A further limitation, due to the small angle of attack or side slip assumption, is that the aerodynamic forces do not to change their direction as a function of the actual deformation of the structure and wing-tip deflection. The aerodynamic forces were defined with respect to the local normal direction of each panel by modifying the modulus, but not the orientation, of each aerodynamic force as a function of the local deformation.

The above approximations are general acceptable when applied to conventional aircraft structures subject to small deformations, and indeed the Doublet Lattice method has been the aeroelastic workhorse of the aerospace industry for over 40 years. Within an industrial environment, aircraft loads estimation requires the computation many tens of thousands of loads cases and as a consequence, high fidelity CFD based analyses cannot be extensively employed. Furthermore unsteady gust analyses using CFD models is still a novel methodology and is very much an immature approach for industrial applications and consequently the Doublet Lattice method is still a standard tool within the industrial community for aircraft loads estimation. Consequently, it was felt acceptable to use this approach to model the effects of the wing-tip device, particularly as the rotations and deflections are not large.

In order to allow for simulation in the time domain, the aerodynamic matrices were transformed using the rational function approximation method proposed by Roger [15]. Following some manipulation, and taking into account the static aerodynamic forces due to a prescribed trim angle of attack α, the aerodynamic loads can be formulated in the time domain as

$$M_{aero} = q_{dyn}\left\{\left[Q_0(\theta-\theta_{\alpha_{0L}})+\frac{c}{2V}Q_1\dot{\theta}+\left(\frac{c}{2V}\right)^2 Q_2\ddot{\theta}\right]+\left[Q_{g0}w+\frac{c}{2V}Q_{g1}\dot{w}+\left(\frac{c}{2V}\right)^2 Q_{g2}\ddot{w}\right] + \sum_{l=1}^{N_{Poles}} R_l + Q_{\alpha 0}(\alpha-\alpha_{0L})\right\} \tag{18}$$

where R_l is the generic aerodynamic state vector related to the generic lag-pole $\left(b_l=\frac{k_{max}}{l}\right)$. These extra states allow the unsteady response of the aerodynamics to be modelled taking into account the delay of the aerodynamic forces with respect to the structural deformations. These aerodynamic states were evaluated through the set of dynamic equations

$$\dot{R}_l = -b_l\frac{2V}{c}IR_l + Q_{2+l}\dot{\theta}+Q_{g2+l}\dot{w} \qquad l=1,\ldots,N_{Poles} \tag{19}$$

Here, a zero zero-lift angle of attack $\alpha_{0L}=0$ was assumed, a non-zero value could be defined to take into account the effect of any wing-tip camber. From Eq. (1), the $\alpha=\alpha_{0L}$ condition is given for an angle of rotation of $\theta=\theta_{\alpha_{0L}}=-\tan^{-1}\left(\frac{\tan\alpha_{0L}}{\sin\Lambda}\right)$.

The generic aerodynamic matrices Q and Q_g are a strict function of hinge angle Λ and Fig. 11 shows the trend of the aerodynamic stiffness terms Q_0 and $Q_{\alpha 0}$. When the hinge is rotated inboard ($\Lambda < 0$) the aerodynamic stiffness Q_0 is positive, leading to a positive aerodynamic forces for an upward rotation of the wing-tip. Such a design leads to a statically unstable system which also reduces the loads alleviation capability as, following a gust event, the wing-tip would have a positive rotation and the generated upward aerodynamic forces would give a further increase of the overall loads. For these reasons only outboard rotated hinges enable loads alleviation.

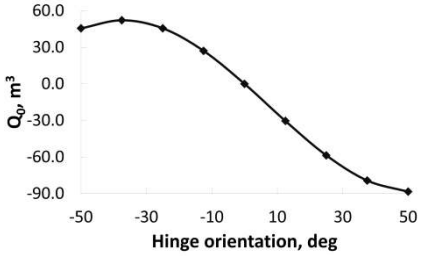

(a) $Q_0(\Lambda)$.

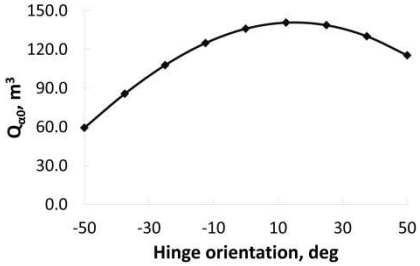

(b) $Q_{\alpha 0}(\Lambda)$.

Figure 11. Aerodynamic Stiffness vs Hinge Orientation

C. Equation of Motion

The nonlinear dynamic equation motion for the system is described as

$$I_\theta \ddot{\theta} + D_\theta \dot{\theta} + K_\theta(\theta - \theta_0) + M_{nl} = M_{aero} + mgd_{CG}\cos\theta \tag{20}$$

where θ_0 is the initial wing-tip deflection, I_θ is the moment of inertia of the structure, D_θ is the hinge damping coefficient, K_θ is the linear hinge spring stiffness, M_{nl} is the nonlinear moment provided by the oblique springs, M_{aero} is the aerodynamic moment and $mgd_{CG}\cos\theta$ represents the moment due to the gravity, where d_{CG} is the distance of the center of gravity from the hinge. Both d_{CG} and I_θ are functions of the hinge orientation Λ and the mass distribution of the folding device. This paper focuses on the structural design of the nonlinear hinge spring, so the effect of the mass and the hinge orientation, already discussed previously [1], were not investigated. For all the presented results it is assumed that $m = 100\,Kg$ and $\Lambda = 25°$.

Recasting Eq. (9) as a single degree of freedom model leads to the overall static aeroelastic hinge moment such that

$$M_{tot} = M_{struct} - q_{dyn}Q_0\left(\theta - \theta_{\alpha_{0L}}\right) - q_{dyn}Q_{\alpha 0}(\alpha - \alpha_{0L}) - mgd_{CG}\cos\theta \tag{21}$$

whose related aeroelastic stiffness is given by

$$K_{tot} = K_{struct} - q_{dyn}Q_0 + mgd_{CG}\sin\theta \tag{22}$$

where $q_{dyn}Q_0$ represents the aerodynamic stiffness $K_{aero\theta}$ of Eqs. (9) and (10).

Equation (21) highlights how the static aeroelastic hinge moment is not only a function of the structural design parameters but also of the flight condition. In particular, the term $q_{dyn}Q_{\alpha 0}(\alpha - \alpha_{0L})$ represents the static load contribution due to the dynamic pressure and the angle of attack that can affect the number of equilibrium points of the system for a given structural design. The equilibrium points of the complete aeroelastic system are given by the roots of the static aeroelastic hinge moment shown in Eq. (21). Figure 12 shows the qualitative evolution of M_{tot} for two different generic structural designs by keeping the dynamic pressure fixed and varying the angle of attack $\alpha: 0° \rightarrow 8°$. The general effect is a shift in the downwards direction of the moment curve with an increment of α, which could lead the system to pass from having only one equilibrium point to three equilibrium points, as shown in Fig. 12(b). This kind of bifurcation may arise only for those structural designs and dynamic pressures that allow negative aeroelastic stiffness K_{tot} for a range of rotation angles θ.

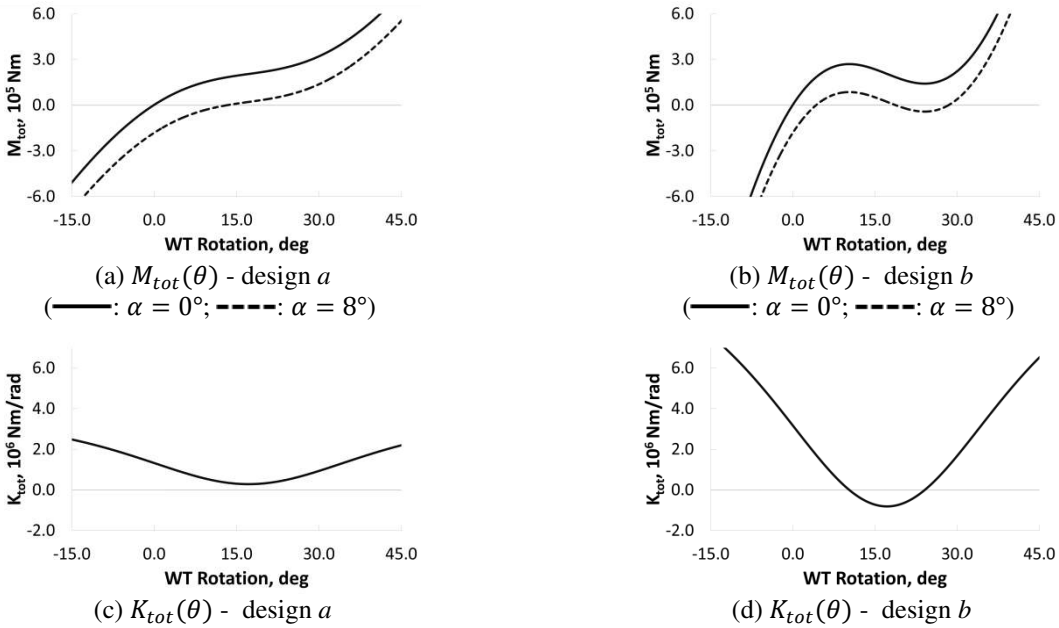

(a) $M_{tot}(\theta)$ - design a (——: $\alpha = 0°$; - - - -: $\alpha = 8°$)

(b) $M_{tot}(\theta)$ - design b (——: $\alpha = 0°$; - - - -: $\alpha = 8°$)

(c) $K_{tot}(\theta)$ - design a

(d) $K_{tot}(\theta)$ - design b

Figure 12. Effect of Angle of Attack α on the System's Equilibrium Points

D. Results

Several aeroelastic analyses were performed in order to investigate the dynamic response of the folding wing-tip for different structural designs. As the structural model is nonlinear, it is not possible to evaluate the static and dynamics responses separately and then superimpose their effects, consequently, the dynamic gust response analyses were performed starting from the trimmed flight configuration. A "1-g" load case was considered with the wing-tip operating at $M = 0.6$ at $25{,}000\ ft$, equivalent to a dynamic pressure of $9.47\ KPa$ and at an angle of attack of $\alpha = 6.25°$. Several aeroelastic analyses were then made over a range of gust lengths. With reference to Eq. (17), w_{ref} was varied linearly from $13.4\ m/s$ EAS at $15{,}000\ ft$ to $7.9\ m/s$ EAS at $50{,}000\ ft$, based on the FAA Federal Aviation Regulations. At the investigated flight altitude of $25{,}000\ ft$ and Mach number $M = 0.6$, the gust reference velocity was $11.48\ m/s$ EAS, while the gust lengths varied between $18\ m$ and $214\ m$.

1. Linear Hinge Model

Since a single degree of freedom model was considered, the hinge moment was the only load information that could be retrieved. As the loads were given mainly by the balance of gust, aerodynamic and inertial vertical forces acting on the wing-tip, it was assumed that the trend of the global hinge moment would reflect qualitatively the contribution of the wing-tip on the wing root bending moment when a full aircraft model was considered. Following on from the findings of previous work [1], an outboard rotated hinge low wing-tip mass with no damping and negligible spring stiffness were used.

Figures 13 and 14 show maximum incremental loads and the wing-tip deflections due to a family of "1-cosine" gusts for four structural configurations with the same mass $m = 100\ Kg$, hinge angle $\Lambda = 25.°$, no hinge damping element, but different initial deflections and spring stiffness as reported in Table 1, where the stiffness of the two latter configurations was defined according to Eq. (11). As expected, maximum loads were experienced by the fixed hinge model while, for the other configurations, a lower hinge stiffness led to lower resulting loads. In particular, it was found in Fig. 14(a) that setting $K_\theta \approx 0.\ Nm/rad$ provided the best loads alleviation as the gusts did not provide any further increment to the hinge moment; the drawback was the significant wing-tip deflection due to the static aerodynamic trim loads, leading to a consequent worsening of the trim aerodynamic performance. An intermediate solution can be found by employing a spring stiffness as defined by Eq. (11) for a given θ_0 and flight condition.

Figure 15 shows the time histories of the hinge moment for the same structural configurations and a fixed gust length of $L_g = 104.m$. It is demonstrated how a very low spring stiffness $K_\theta \approx 0.\ Nm/rad$ allows the wing-tip to deflect enough to generate negative lift to balance the positive gust contribution, whereas a higher spring stiffness leads to a lower deflection resulting in a worse loads alleviation performance.

Configurations:	$\theta_0\ [deg]$	$K_\theta\ [Nm/rad]$
Hinge-Fixed	0.	∞
Hinge-Free	0.	0.
Hinge-A	$-25.$	$3.217E05$
Hinge-B	-12.5	$6.434E05$

Table 1. SDOF Linear Hinge Model – Structural Configurations

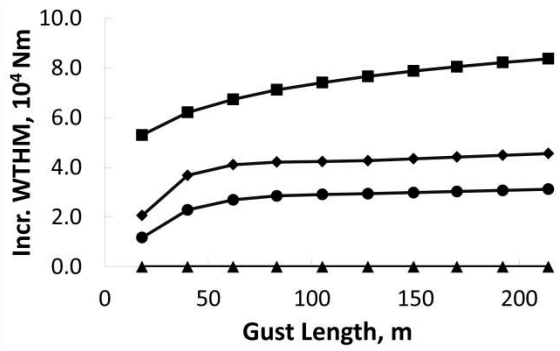

Figure 13. Linear Gust Response - Maximum Incremental Wing-Tip Hinge Moments vs Gust Lengths (■: Hinge-Fixed; ▲: Hinge-Free; ●: Hinge-A; ◆: Hinge-B)

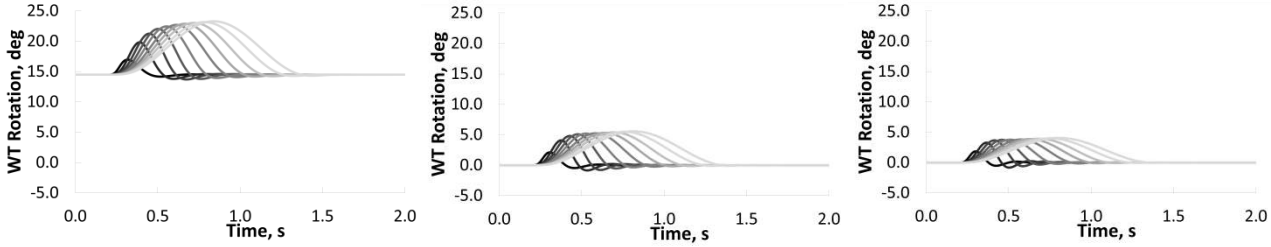

(a) Hinge-Free (b) Hinge-A (b) Hinge-B

Figure 14. Linear Gust Response - Wing-tip Deflection vs Time

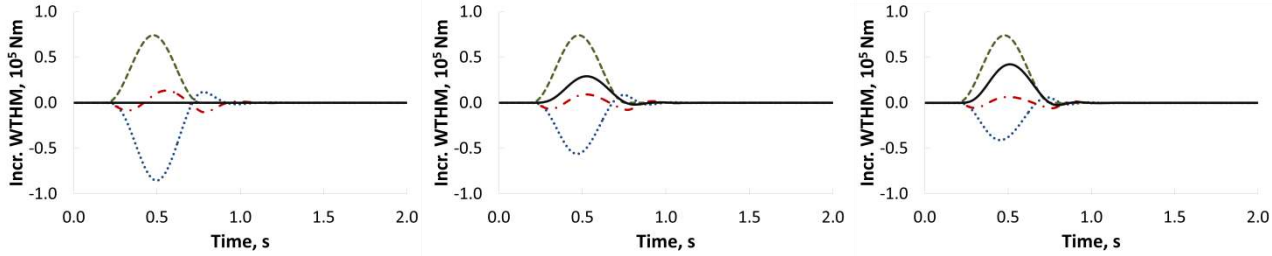

(a) Hinge-Free (b) Hinge-A (b) Hinge-B

Figure 15. Incremental Linear Unsteady Gust Loads vs Time for $L_g = 104.m$ (- - - -: gust loads; ·····: aerodynamic loads due to the wing-tip deflection; — · —: inertial loads; ——: global loads)

2. Nonlinear Hinge Model

Several structural configurations were considered, varying the hinge device design parameters according the high static low dynamic aeroelastic stiffness concept introduced in the previous section. Table 2 shows the four

different nonlinear spring designs that have been considered. In combination with the linear models of the previous section "Hinge-A" and "Hinge-B", two sets of oblique springs with an inclination of $\sigma_0 = 30.°$ ($\gamma = 0.866$) and $\sigma_0 = 60.°$ ($\gamma = 0.5$) were defined. The related non-dimensional pulley radii $\hat{r}$ were defined according Eq. (12). For each of the four configurations the spring stiffness ratio ν was then varied between the values ν_{qzas} and ν_{qzss}.

Configurations:	$\theta_0\ [deg]$	$K_\theta\ [Nm/rad]$	γ	$\hat{r}$	ν
Hinge-A1	$-25.$	$3.217E05$	0.866	1.15	$[3.23, 4.63, 6.02, 7.42, 8.81]$
Hinge-A2	$-25.$	$3.217E05$	0.5	1.98	$[0.5, 0.72, 0.93, 1.15, 1.36]$
Hinge-B1	-12.5	$6.434E05$	0.866	2.92	$[3.23, 3.93, 4.63, 5.32, 6.02]$
Hinge-B2	-12.5	$6.434E05$	0.5	3.96	$[0.5, 0.61, 0.72, 0.82, 0.93]$

Table 2. SDOF Nonlinear Hinge Model – Structural Configurations

Figure 16 shows the loads envelope obtained for different gust lengths and the overall moment and stiffness for the "Hinge-A1". The higher that ν was set, the lower the stiffness of the system at the equilibrium point and so the better the loads alleviation performance. In particular, the loads were always lower than those of the linear configuration "Hinge-A". Furthermore, for such a configuration $\nu_{qzss} = 3.23$ and $\nu_{qzas} = 8.81$, it can be seen that when $\nu = \nu_{qzss}$ the overall aeroelastic stiffness of the nonlinear model was equal locally to that of the linear system when $K_\theta \approx 0. Nm/rad$ (dotted line Fig. 16(c)) around the equilibrium point, leading the wing-tip to experience an almost zero incremental hinge moment during a gust event. When $\nu_{qzss} < \nu < \nu_{qzas}$ the aeroelastic stiffness of the system was even lower than that of the linear system with $K_\theta \approx 0. Nm/rad$, allowing negative values of the maximum hinge moment despite the positive gust loads.

A better understanding of the system response can be found by examining the time histories of the loads for this configuration, for gust length, $L_g = 104. m$, and for different values of ν, as shown in Fig. 17. When $\nu = 3.23$ the folding device generates just enough negative lift variation to balance the positive gust increment; when $\nu = 6.02$, the lower aeroelastic stiffness allowed higher wing-tip rotations and so the generation of negative aerodynamic forces that overcame the positive gust loads and this trend is even more emphasized for $\nu = 8.81$. The drawback in using a higher value of ν is that the folding device needs a longer time to recover the undeflected trim configuration because of the very low stiffness value, as seen by the slower decay of the negative lift contribution due to the wing-tip deflection in Fig. 17(c) (dotted line).

Figure 18 shows a comparison between the displacements of the linear and nonlinear models sharing the same linear torsional spring, demonstrating that the nonlinear springs enable higher rotations and hence a better loads alleviation, whilst still allowing the system to recover the original undeflected configuration after the gust event.

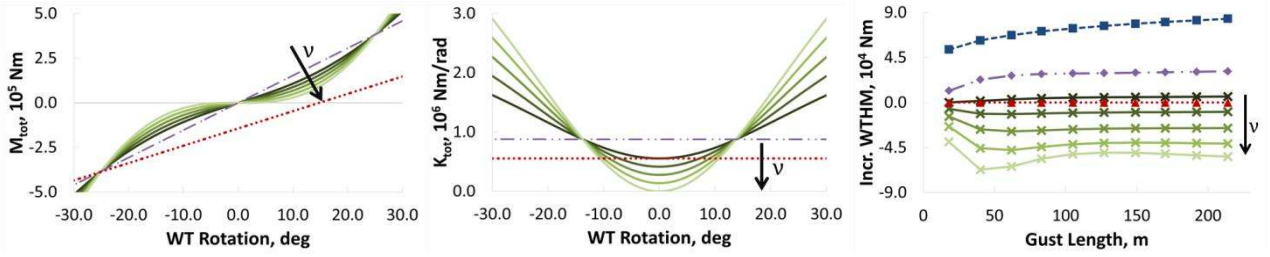

(a) $M_{tot}(\theta)$ (b) $K_{tot}(\theta)$ (c) Loads Envelope vs Gust Lengths

Figure 16. Nonlinear Gust Response – Hinge-A1
(– – – –: Hinge-Fixed; — · · : linear model Hinge-A;
·····: linear model Hinge-Free; ——: nonlinear model Hinge-A1)

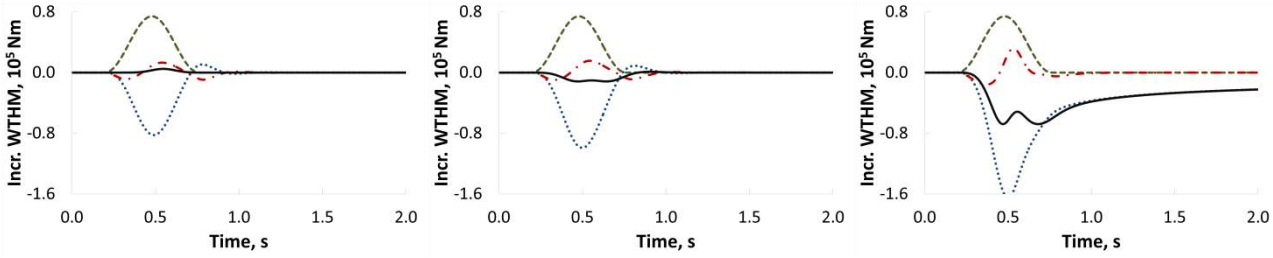

(a) $\nu = 3.23$ (b) $\nu = 6.02$ (c) $\nu = 8.81$

Figure 17. Incremental Unsteady Gust Loads vs Time for $L_g = 104.m$ – Hinge-A1
(- - - -: gust loads; ·····: aerodynamic loads due to the wing-tip deflection; – · – ·: inertial loads; ——: global loads)

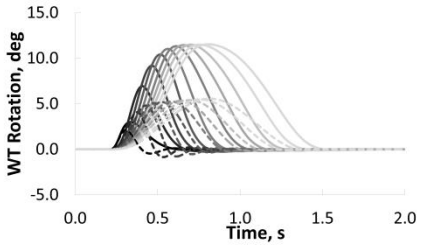

Figure 18. Linear vs Nonlinear Gust Response – Hinge-A1 ($\nu = 6.02$)
(- - - -: linear model; ——: nonlinear model)

Figure 19 shows the loads envelope for different gust lengths and the overall moment and stiffness for the "Hinge-A2" configuration. The comments related to the previous case remained valid also for this configuration, with only a slight worsening on the loads alleviation performance. This effect is due to the higher radius $\hat{r}$ which causes the oblique springs to provide a negative stiffness contribution over a smaller range of rotation angles θ.

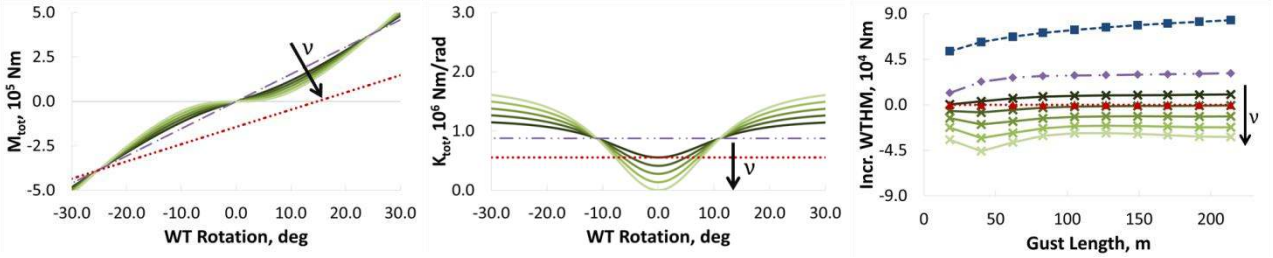

(a) $M_{tot}(\theta)$ (b) $K_{tot}(\theta)$ (c) Loads Envelope vs Gust Lengths

Figure 19. Nonlinear Gust Response – Hinge-A2
(- - - -: Hinge-Fixed; — · · : linear model Hinge-A;
·····: linear model Hinge-Free; ——: nonlinear model Hinge-A2)

Figures 20 and 21 show the loads envelope for different gust lengths and the overall moment and stiffness when "Hinge-B2" and "Hinge-B1" configurations were employed. For both cases it can be seen that the loads of the nonlinear models were lower than those of the linear model "Hinge-B". Even though the designs with the higher stiffness ratios ν allowed very low stiffness values around the equilibrium point, the hinge moment envelopes exhibit loads that were always positive and higher than the ones of the linear model with $K_\theta \approx 0. Nm/rad$.

Again, this worsening in the alleviation performance for this latter case can be attributed to the higher $\hat{r}$ employed. Equations (11) and (12) show that the higher the initial wing-tip deflection θ_0 and the lower the initial oblique springs inclination ($\gamma \to 1.$), the lower the resulting linear spring stiffness K_θ and pulley radius $\hat{r}$. The latter

term is a fundamental parameter for the definition of the nonlinear contribution of the oblique springs; the lower that $\hat{r}$ is, the higher the wing-tip rotation needed to produce the same oblique spring's horizontal displacement. Therefore, the nonlinear effects are spread over a longer range of folding angles leading to a smoother reduction of the aeroelastic stiffness. Once the geometry of the hinge device is fixed, the spring stiffness ratio ν can be used as a tuning parameter to control the reduction of the aeroelastic stiffness around the equilibrium point. The red dotted lines in Figs. 16(b) and 19-21(b), represent the aeroelastic stiffness of the linear hinge device with $K_\theta = 0. Nm/rad$, therefore they are purely characterized by the aerodynamic stiffness contribution and constitute the zero structural stiffness threshold. When $\nu > \nu_{qzss}$ the system presents a negative structural stiffness, which means K_{tot} is below the zero structural stiffness threshold, over the range of folding angles $\Delta\theta_{nss}$. Within $\Delta\theta_{nss}$ the structural hinge device generated a moment that can be exploited to allow faster and higher wing-tip rotation with respect to the linear model. The value of $\Delta\theta_{nss}$ is mainly a function of $\hat{r}$ and ν; the lower that $\hat{r}$ and the higher that ν are, the higher $\Delta\theta_{nss}$ as it can be seen by comparing Fig. 16(b) and Fig. 20(b), characterized respectively by $\hat{r} = 1.15$ and $\hat{r} = 3.96$.

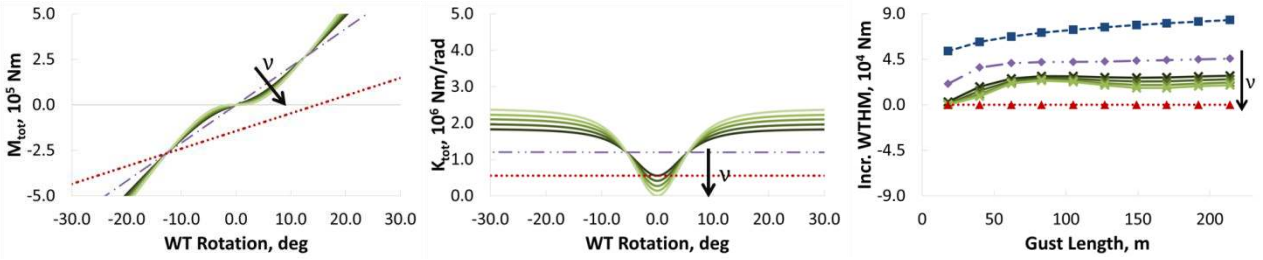

(a) $M_{tot}(\theta)$ (b) $K_{tot}(\theta)$ (c) Loads Envelope vs Gust Lengths

Figure 20. Nonlinear Gust Response – Hinge-B2
(– – – –: Hinge-Fixed; — · · : linear model Hinge-B;
·····: linear model Hinge-Free; ——: nonlinear model Hinge-B2)

The effect of the non-dimensional radius $\hat{r}$ is highlighted in Fig. 22 which shows the time histories of the loads of the "Hinge-B1" design, for given gust length $L_g = 104. m$. When the wing-tip is hit by a gust, the low aeroelastic stiffness value allows fast rotation of the device due to the small local stiffness. The high values of $\hat{r}$ leads the structural stiffness to have a sudden increment after a small deflection of the device, therefore the wing-tip is not slowed down by the negative aerodynamic forces, but by the hinge structural stiffness increment. This results in a sudden stop of the folding device and so the generation of a positive peak of the inertial loads which, combined with the gust moments, overcomes the negative contribution due to the wing-tip rotation. Such behavior is more pronounced for higher values of ν.

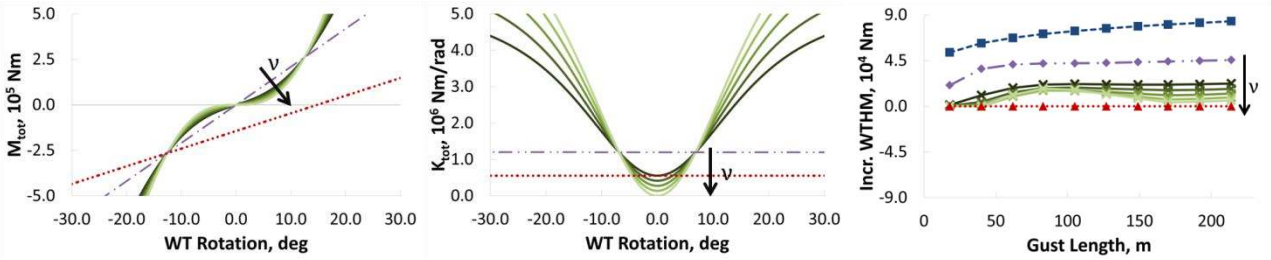

(a) $M_{tot}(\theta)$ (b) $K_{tot}(\theta)$ (c) Loads Envelope vs Gust Lengths

Figure 21. Nonlinear Gust Response – Hinge-B1
(– – – –: Hinge-Fixed; — · · : linear model Hinge-B;
·····: linear model Hinge-Free; ——: nonlinear model Hinge-B1)

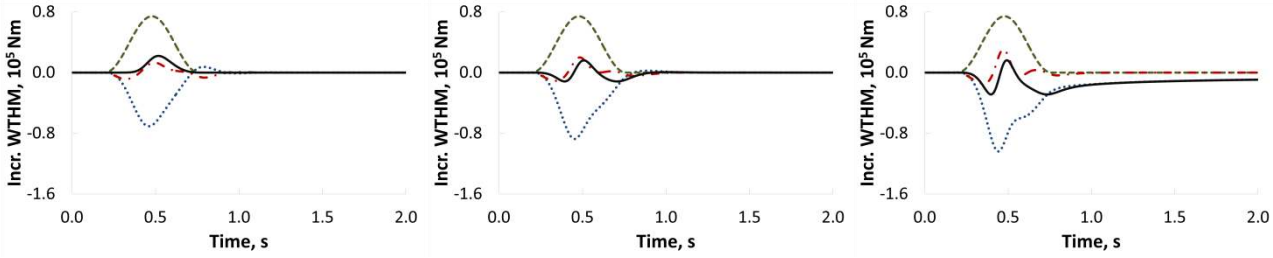

(a) $\nu = 3.23$ (b) $\nu = 4.63$ (c) $\nu = 6.02$

Figure 22. Incremental Unsteady Gust Loads vs Time for $L_g = 104.m$ – Hinge-B1 (- - - -: gust loads; ·····: aerodynamic loads due to the wing-tip deflection; – · –: inertial loads; ——: global loads)

IV. Full Aircraft Model

An investigation of the application of the high static low dynamic aeroelastic stiffness hinge device applied on a full aircraft model is now presented. The purpose is an understanding of the dynamic response of the proposed device when the dynamic coupling of the wing-tip and main airframe is also considered and how this affects the design of the hinge spring.

The same aeroelastic framework used previously [3] was employed for the full aircraft model investigations, but now with the introduction of the high static low dynamic aeroelastic stiffness hinge device. The numerical structural model used for these investigations, involved a $100\ Kg$ wing-tip model with a 25° hinge angle.

For the full aircraft model the overall static aeroelastic hinge moment and stiffness in Eqs. (9) and (10) can be expressed as

$$M_{tot} = M_{struct} - K_{aero\theta}\theta - K_{aero\alpha}\alpha - K_{aero\delta_e}\delta_e - M_g \tag{23}$$

$$K_{tot} = K_{struct} - K_{aero\theta} \tag{24}$$

where $K_{aero\alpha}\alpha$ and $K_{aero\delta_e}\delta_e$ are the static aerodynamic hinge moments for a given angle of attack and elevator deflection, and M_g represents the contribution of gravity. Such external loads also generate a static deformation of the entire aircraft with a consequent variation of the aerodynamic forces distribution. These flexibility effects cannot be neglected and have been taken into account considering the nonlinear variation of the different load contributions with the dynamic pressure as shown in Fig. 23. Despite the same wing-tip geometry being defined for the single degree of freedom and full aircraft models, the related aerodynamic stiffness differ because of the aerodynamic coupling effects of the wing-tip and airframe aerodynamic panels as well as the wing twisting effects considered in the full aircraft model. The same observation also occurred for the $q_{dyn}Q_{\alpha 0}$ and $K_{aero\alpha}$ terms.

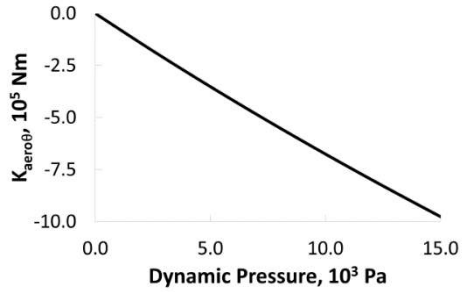

(a) Aerodynamic hinge stiffness

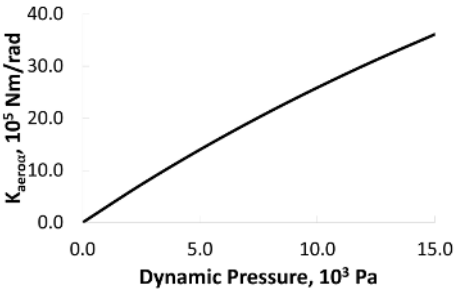

(b) Static aerodynamic hinge moment – α stiffness

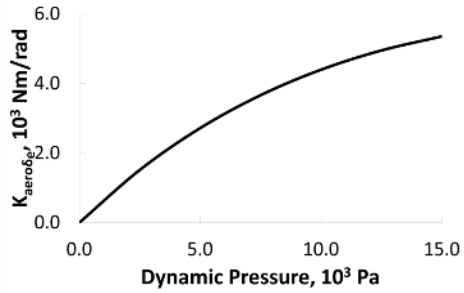

(c) Static aerodynamic hinge moment – δ_e stiffness

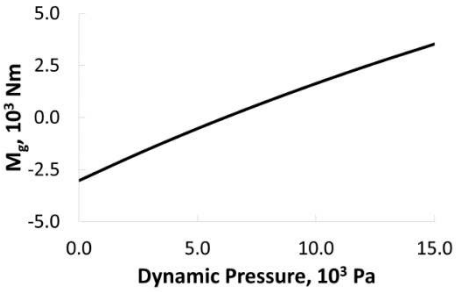

(d) Gravity hinge moment

Figure 23. Hinge Aeroelastic Static Moments Contribution

A. Results

As with the SDOF case, it was not possible to separate the static and the dynamic response due to the nonlinearity of the hinge device, therefore the dynamic gust response analyses were performed starting from a trimmed flight configuration. The same flight condition, in terms of Mach value, altitude and dynamic pressure, and the same "*1-cosine*" gusts family considered for the single degree of freedom model were defined for the full aircraft model as well.

Several structural configurations were considered by varying the hinge device design parameters according the high static low dynamic aeroelastic stiffness concept introduced in the previous section. All the investigated hinge device designs that satisfied the condition $\theta_{trim} = 0°$ led to the same trim flight condition given by an angle of attack of $6.25°$ and elevator deflection of $-12.39°$. Figure 24 shows an example of the different structural configurations between the initial and trimmed flight conditions.

Table 3 reports the spring designs that have considered for the nonlinear gust response analyses: two different wing-tip initial folding angles, with the related linear spring stiffness, defined as in Eq. (11), were selected. For each of these combinations, two sets of oblique springs with an inclination of $\sigma = 30.°$ (i.e. $\gamma = 0.866$) and $\sigma = 60.°$ (i.e. $\gamma = 0.5$) were specified; the related non-dimensional pulley radii $\hat{r}$ were defined according Eq. (12). Finally, ν was varied for each structural configuration between the related ν_{qzss} and ν_{qzas} values.

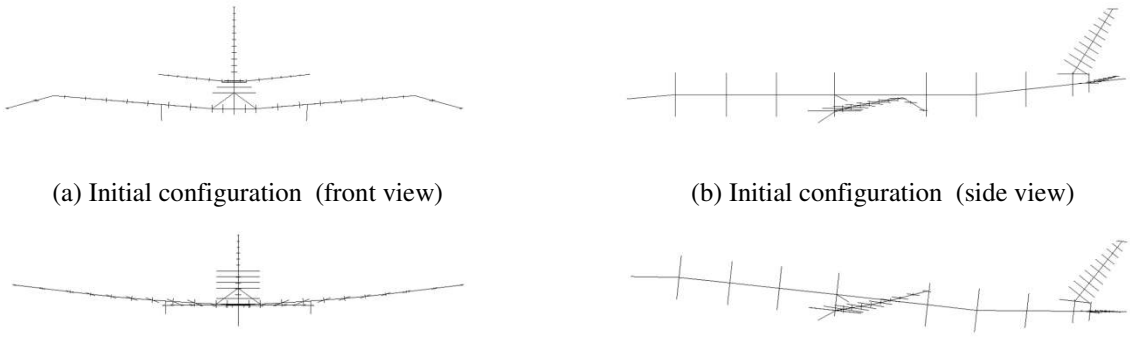

(a) Initial configuration (front view) (b) Initial configuration (side view)

(c) Trim configuration (front view) (b) Trim configuration (side view)

Figure 24. Static Trim Deformation

Configurations:	$\theta_0\ [deg]$	$K_\theta\ [Nm/rad]$	γ	$\hat{r}$	ν
Hinge-L	-12.5	$1.237E06$	-	-	-
Hinge-L1	-12.5	$1.237E06$	0.5	3.70	$[0.5, 0.56, 0.63, 0.69, 0.76]$
Hinge-L2	-12.5	$1.237E06$	0.866	2.29	$[3.23, 3.65, 4.07, 4.49, 4.91]$
Hinge-M	$-25.$	$6.186E05$	-	-	-
Hinge-M1	$-25.$	$6.186E05$	0.5	1.98	$[0.5, 0.63, 0.76, 0.89, 1.01]$
Hinge-M2	$-25.$	$6.186E05$	0.866	1.15	$[3.23, 4.07, 4.91, 5.75, 6.58]$

Table 3. Full Aircraft Nonlinear Hinge Model – Structural Configurations

Figures 25-28(a) show the aeroelastic stiffness curves as a function of the wing-tip folding angle for the different structural designs. As for the single degree of freedom model, the lower the value of $\hat{r}$, the higher the range of rotations $\Delta\theta_{nss}$ over which the structural hinge device generated a moment so that the folding angle can be exploited to allow faster and higher wing-tip rotation and so enhance the loads alleviation performance with respect to the linear model.

Figures 25-28(b) show the incremental gust loads envelope for different gust lengths for the different structural designs. All the investigated designs allowed a reduction of the maximum loads with respect to the fixed hinge model; for the design "Hinge-L1" and "Hinge-L2", Figs. 25(b) and 26(b), the loads were always higher than the ones of the baseline model and presented only a slight reduction for increasing values of ν; for the "Hinge-M1" and "Hinge-M2" designs the maximum loads were always equal or lower than the baseline model and higher values of ν enabled better alleviation performance.

The reported results highlight again how the loads alleviation capabilities are not only function of the value of the aeroelastic stiffness at the static equilibrium point, but also of the range of rotation $\Delta\theta_{nss}$ over which the structural stiffness is kept negative. When the gust hits the aircraft, all the investigated hinge designs allow a fast wing-tip rotation given the low aeroelastic stiffness K_{tot} at $\theta_{trim} = 0.°$. When high values of $\hat{r}$ were defined, as for the "Hinge-L1" and "Hinge-L2" designs, Figs. 25 and 26, the aeroelastic stiffness shows a sudden increment after a small deflection of the device. As a result, the system experienced lower wing-tip deflections, and therefore can generate a lower negative lift contribution to counteract the positive gust loads; furthermore the sudden braking of the device generates a positive peak of the inertial loads which reduced the loads alleviation capabilities. Lower values of $\hat{r}$, as in Figs. 27 and 28, ensure that the system doesn't suffer such a limitation in its loads alleviation capabilities.

Regarding the minimum loads, they were always larger than those of the baseline model and in some case even higher than those of the fixed hinge model. Nevertheless structural sizing and loads assessment require the combination of the positive static trim loads with those from the incremental gust, as a consequence the positive gust loads, which were reduced by the wing-tip device, are the most critical for the structure.

A better understanding of the system response can be found looking at the time histories of the wing-tip deflections and incremental wing root bending moments, as seen in Figs. 26(c, d) and 28(c, d) for the different

structural configurations and a gust length of $214\ m$, which was the one that generated the highest hinge moments and wing-tip deflections. To allow a more direct comparison of the deflections induced by the gusts for the different models, Figs 26(c) and 28(c) shows the actual wing-tip deflections for the nonlinear models (solid lines), and only the incremental rotations for the linear model with $K_\theta = 0. Nm/rad$ (dotted lines), being for such configuration $\theta_{trim} = 26.96°$. It can be seen that high ν and low $\hat{r}$ minimize K_{tot} and maximize $\Delta\theta_{nss}$ leading to good loads alleviation performance via higher and faster rotations. The structural configuration reported in Figs. 25 and 26 were characterized by a very high $\hat{r}$, respectively 3.70 and 2.29, and low $\Delta\theta_{nss}$; the sudden increment of the aeroelastic stiffness allowed wing-tip rotations lower than the incremental deflections of the linear model, as in Fig. 26(c), therefore the wing root bending moments were lower than those of the fixed hinge model, but higher than the baseline model. The other structural designs, in Figs. 27 and 28, experienced wing-tip deflections equal or higher than those of the linear model with $K_\theta = 0. Nm/rad$ and maximum wing root bending moments equal or lower than the baseline model. The negative stiffness contribution due to the nonlinear oblique springs allowed higher wing-tip deflections resulting in the generation of a negative lift that overcame the gust loads, leading the wing-tip to generate overall negative incremental loads and so leading the aircraft to experience incremental gust loads lower than those of the baseline model.

For $\nu \approx \nu_{qzss}$ the analyzed nonlinear models were characterized by an aeroelastic stiffness close to that of the linear model with $K_\theta = 0. Nm/rad$ in the neighborhood of the equilibrium position $\theta_{trim} = 0.°$, which led to very similar, if not equal, trend of the incremental wing root bending moment and wing-tip gust responses.

For all the investigated designs, high values of ν enabled a low aeroelastic stiffness leading to a reduction of the positive gust loads because of the fast upward wing-tip rotation. However, due to the low aeroelastic stiffness, the wing-tip needed more time to recover the original undeflected configuration, as shown in Figs. 26(c) and 28(c). Such slower wing-tip dynamics, following the initial gust positive peak, led to a delay of the wing-tip response with respect the wing root bending moment which is the main reason behind the worsening of the loads alleviation capabilities for negative gust loads [1]. Moreover, for all the investigated designs when $\nu \approx \nu_{qzas}$ the wing-tips were not able to recover the original undeflected configuration after the gust. The aeroelastic stiffness of the system was too small to balance the variation of the static loads acting on the hinge due to the variation of the angle of attack after the gust. Such an effect could not be captured by the single degree of freedom model since the angle of attack was considered as a constant value during the simulation, and no rigid pitch or heave motion of the wing-tip device were taken into account.

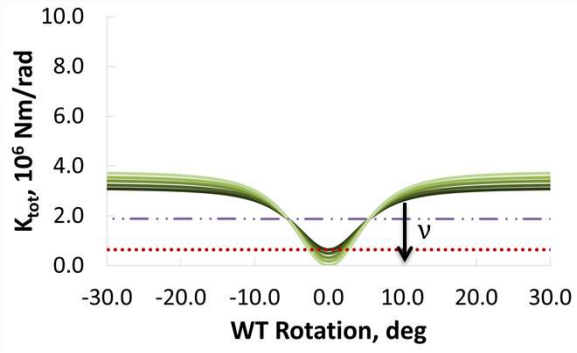

(a) $K_{tot}(\theta)$

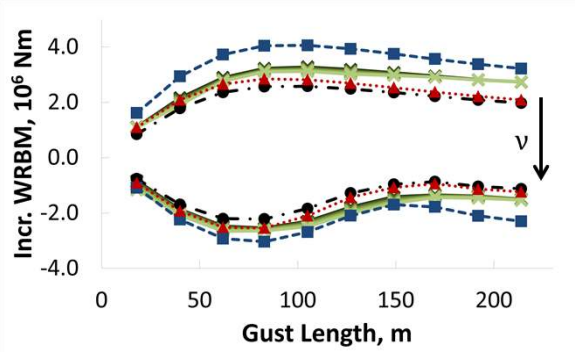

(b) Loads Envelope vs Gust Lengths

Figure 25. Nonlinear Gust Response – Hinge-L1
(– · –: baseline model; – – –: Hinge-Fixed; — · · : linear model Hinge-L; ·····: linear model Hinge-Free; ——: nonlinear model Hinge-L1)

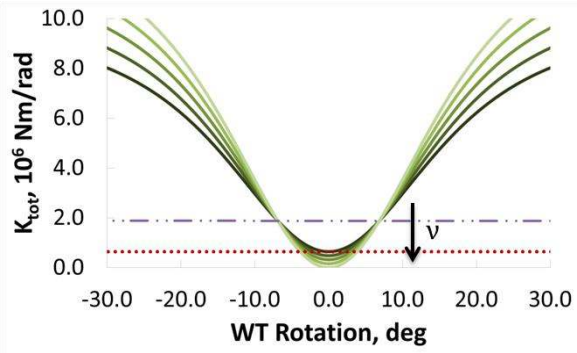

(a) $K_{tot}(\theta)$

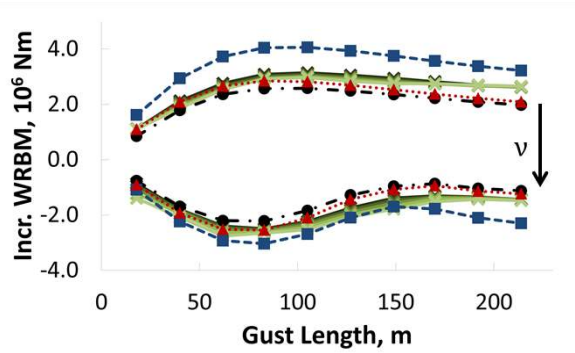

(b) Loads Envelope vs Gust Lengths

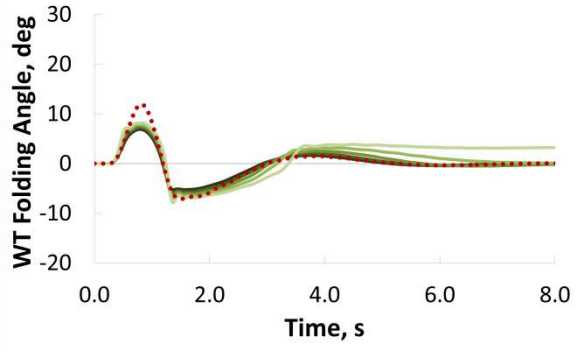

(c) Wing-tip folding angle - time histories for *Lg=214 m*

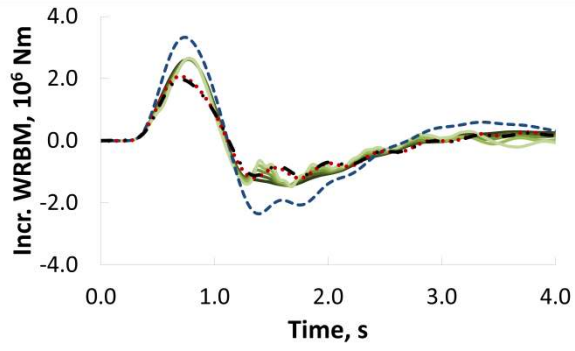

(d) Incremental WRBM - time histories for *Lg=214 m*

Figure 26. Nonlinear Gust Response – Hinge-L2
(– · –: baseline model; – – –: Hinge-Fixed; — · · : linear model Hinge-L; ·····: linear model Hinge-Free; ——: nonlinear model Hinge-L2)

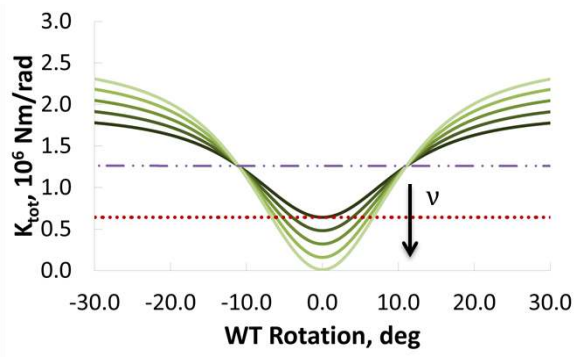

(a) $K_{tot}(\theta)$

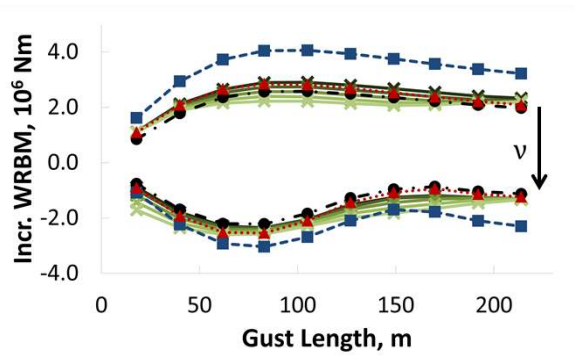

(b) Loads Envelope vs Gust Lengths

Figure 27. Nonlinear Gust Response – Hinge-M1
(– · –: baseline model; - - - -: Hinge-Fixed; — · · : linear model Hinge-M; ·····: linear model Hinge-Free; ——: nonlinear model Hinge-M1)

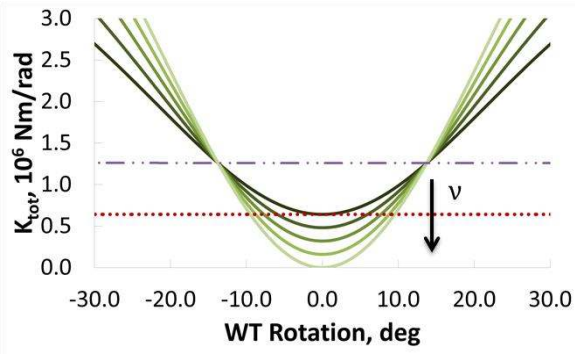

(a) $K_{tot}(\theta)$

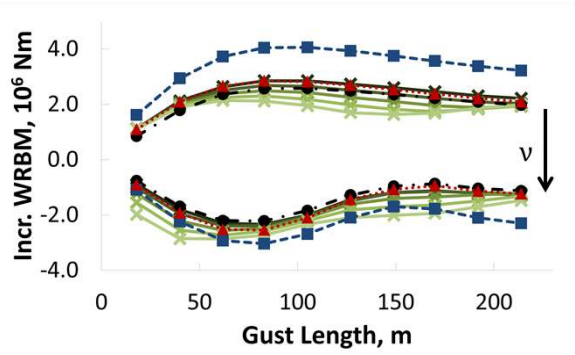

(b) Loads Envelope vs Gust Lengths

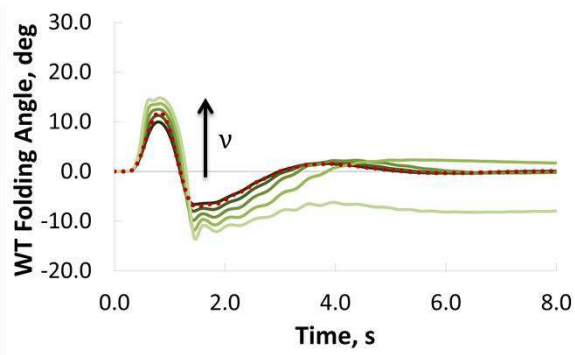

(c) Wing-tip folding angle - time histories for *Lg=214 m*

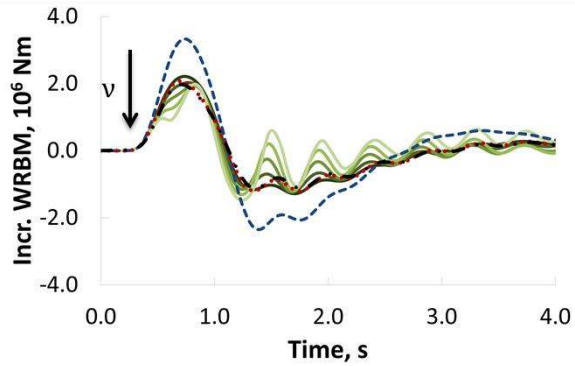

(d) Incremental WRBM - time histories for *Lg=214 m*

Figure 28. Nonlinear Gust Response – Hinge-M2
(– · –: baseline model; - - - -: Hinge-Fixed; — · · : linear model Hinge-M; ·····: linear model Hinge-Free; ——: nonlinear model Hinge-M2)

V. Conclusions

A preliminary investigation into the use of nonlinear negative stiffness folding wing-tips as a gust loads alleviation device was performed using a single degree of freedom wing-tip model and a representative civil jet aircraft aeroelastic model. A wing-tip device was connected to the wings with a hinge and the effect of a nonlinear hinge device on the response to "1-cosine" gusts was investigated. All results were related to the loads acting on a baseline model which consisted of the aircraft without wing-tips, i.e. 20% less span.

A high static low dynamic aeroelastic stiffness mechanism was designed to allow a device stiff enough to keep the wing-tip undeflected during the cruise, while allowing fast and significant deflections in the case of a vertical gust with consequent reduction of the incremental loads.

The use of a nonlinear spring device enabled an improvement in loads alleviation capabilities compared to the linear device, reducing the incremental wing root bending moments to smaller levels compared to those of the baseline model. It was proven that significant loads alleviation were possible when the system exhibited a low overall stiffness around the trim equilibrium point for a large enough range of deflection angles. The negative stiffness contribution of the oblique springs allowed higher and faster wing-tip deflections resulting in a reduction of the gust effect. Moreover, the passive hinge device designs allowed the folding device to recover the original undeflected configuration after the gust.

Through proper design of the wing-tip device it will be possible to increase the wing aspect ratio with little, if any, increase or even a reduction of the gust loads experienced by the aircraft, leading to better aerodynamic efficiency and/or reduced structural weight on existing platforms.

VI. Acknowledgments

The research leading to these results has received funding from the European Community's Marie Curie Initial Training Network (ITN) on Aircraft Loads Prediction using Enhanced Simulation (ALPES) FP7-PEOPLE-ITN-GA-2013-607911 and also the Royal Academy of Engineering. The partners in the ALPES ITN are the University of Bristol, Siemens PLM Software and Airbus Operations Ltd.

References

[1] Castrichini, A.,Hodigere Siddaramaiah., V., Calderon., D.E., Cooper, J.E., Wilson, T., Lemmens, Y., "Preliminary Investigation of Use of Flexible Folding Wing-Tips for Static and Dynamic Loads Alleviation", *4th RAeS Aircraft Structural Design Conference,* Belfast, 2014.

[2] Khodaparast H.H, Cooper J.E., "Rapid Prediction of Worst Case Gust Loads Following Structural Modification", AIAA Journal, Vol. 52, No. 2 (2014), pp. 242-254.

[3] Castrichini, A.,Hodigere Siddaramaiah., V., Calderon., D.E., Cooper, J.E., Wilson, T., Lemmens, Y., "Nonlinear Folding Wing Tips for Gust Loads Alleviation", Journal of Aircraft, published online 17 Feb. 2016. Doi: http://dx.doi.org/10.2514/1.C033474

[4] Gatto A., Mattioni F. and Friswell M. I., "Experimental Investigation of Bistable Winglets to Enhance Aircraft Wing Lift Takeoff Capability", Journal of Aircraft, Vol. 46, No. 2 (2009), pp. 647-655.

[5] Arrieta A. F., Bilgen O., Friswell M. I., Hagedorn P., "Dynamic control for morphing of bi-stable composites", Journal of Intelligent Material Systems and Structures, 24(3) 266–273.

[6] Bilgen O.,Arrieta A. F., Friswell M. I., Hagedorn P., "Dynamic control of a bistable wing under aerodynamic loading", Smart Materials and Structures, 22 (2013) 025020.

[7] Carrella, A., Brennan M. J. & Waters T. P., "Static analysis of a passive vibration isolator with quasi-zero-stiffness characteristic." Journal of Sound and Vibration 301.3 (2007): 678-689.

[8] Rivin E.I., "Passive Vibration Isolation", ASME Press, New York, 2001.

[9] Alabuzhev P., Gritchin A., Kim L., Migirenko G., Chon V., Stepanov P., "Vibration Protecting and Measuring Systems with Quasi-Zero Stiffness", Hemisphere Publishing, New York, 1989.

[10] Platus D.L., "Negative-stiffness-mechanism vibration isolation systems", SPIE—Vibration Control in Microelectronics, Optics and Metrology 1619 (1991) 44–54.

[11] Schenk M & Guest S.D., "On zero stiffness", Proceedings of the Institution of Mechanical Engineers, Part C: Journal of Mechanical Engineering Science, 228. pp. 1701-1714. ISSN 0954-406.

[12] Albano E., Rodden W.P., "A Doublet-Lattice Method for Calculating Lift Distributions on Oscillating Surfaces in Subsonic Flows", AIAA Journal v7 n2 1969 pp 279-285.

[13] Rodden W.P., Johnson E.H. , “MSC/NASTRAN Aeroelastic Analysis’ User’s Guide”, MSC Software, USA, 1994.
[14] Wright J.R., Cooper J.E., “Introduction to Aircraft Aeroelasticity and Loads”, John Wiley, 2007.
[15] Roger K.L., “Airplane Math Modeling Methods For Active Control Design”, AGARD Structures and Materials Panel, number CP-228, pp 4-11, 1977.